Advanced Steel Construction – Vol. 21 No. 6 (2025) 530–541
DOI: 10.18057/IJASC.2025.21.6.6

STUDY ON HUMAN-INDUCED VIBRATION OF AN INNOVATIVE SPATIAL CABLE-SUPPORTED FLOOR SYSTEM

Qi An [1, *], Hang-Qi Zheng [1], Yu-Hao Dong [1], Xiu-Jun Wang [2], Yan-Song Diao [1] and Zhong-Hua Wang [2]

[1] *School of Civil Engineering, Qingdao University of Technology, Qingdao 266520, China*
[2] *The Fourth Construction Co., Ltd. of China Construction Eighth Engineering Division, Qingdao 266000, China*
**(Corresponding Author: E–mail: anqi@qut.edu.cn)*

ABSTRACT

The growing demand for expansive indoor spaces in public buildings has necessitated the development of an innovative spatial cable-supported floor system (SCSFS). Experimental results revealed that the first-order natural frequency of the test floor is 17.58 Hz, with a damping ratio of 0.028. Among the four types of loads analyzed, jumping loads induced the most significant human-induced vibration acceleration responses in the floor system, whereas walking loads had a relatively minor impact. Numerical simulations further demonstrated that parameters such as the arrangement of cable-strut system, beam height, cable cross-sectional area, and sag of cable-strut system significantly influence the natural frequency of the floor system. Moreover, these parameters, along with steel beam cross-section type and floor slab thickness, play a critical role in the acceleration response. Conversely, changes in the cross-sectional area of the struts, boundary conditions, and prestress levels were found to have minimal impact on both natural frequency and acceleration responses. This study elucidates the natural vibration characteristics and human-induced vibration mechanisms of the SCSFS, identifies the effects of key structural parameters on human-induced vibration responses, and provides a theoretical and technical foundation for the practical engineering application of SCSFS. The findings possess substantial scientific and engineering value.

ARTICLE HISTORY

Received: 18 March 2025
Revised: 22 July 2025
Accepted: 2 August 2025

KEYWORDS

Spatial cable-supported floor system;
Large-span floor system structures;
Human-induced vibration;
Comfort analysis;
Numerical simulation

1. Introduction

In the field of contemporary architecture, with the increasing complexity of functional requirements and the continuous innovation of spatial concepts, long-span floor systems have become the core structural solution for realizing ultra-large-span column-free spaces.

Compared with small and medium-span floor systems (such as concrete floors, composite floors, and timber floors [1]) which feature diverse forms and mature technologies, the development of long-span floor systems [2-9] still faces significant challenges in terms of structural form innovation and research depth. In engineering practice, long-span requirements are primarily met through four types of floor systems: prestressed concrete floors [10-12], steel truss composite floors [13-15], open-web sandwich floors [16-17], and cable-supported floors [18-20]. However, with the continuous increase in architectural span requirements, the limitations of existing mainstream systems have gradually become apparent: long-span prestressed concrete floors face severe challenges in crack control and excessive self-weight [21]; the load-bearing capacity of steel truss composite floors relies on steel truss systems, which consist of upper chords, lower chords, web members, and other components connected via dense joints, resulting in complex component layouts and low space utilization; open-web sandwich floors have limited spanning capacity; cable-supported floors still require further research and technical breakthroughs in terms of refined node design, construction tension control, and adaptability to complex spatial forms.

Therefore, exploring and developing innovative structural solutions that can more efficiently synergize the performance of different materials, optimize key structural details, and enhance overall stability and space utilization has become a crucial research direction for advancing the development of modern architectural spaces.

In response to these limitations, this study introduces a novel spatial cable-supported floor system (SCSFS) designed for large-span applications [22], as illustrated in Fig. 1. The SCSFS comprises two main components: an upper rigid composite floor system and a lower spatial cable-strut system. The upper rigid composite floor system integrates concrete floor slabs with intersecting steel beams, while the lower spatial cable-strut system includes inner and outer rings, radially arranged cables, and circumferential cables. The lower ends of the struts connect to the radial and circumferential cables, and the upper ends connect to the steel beams via universal rotational nodes.

Compared to existing large-span floor systems, the SCSFS offers several key advantages:

1) It leverages the compressive performance of concrete slabs to bear vertical loads and relies on the tensile properties of cables to transmit horizontal forces. Compared with traditional structures (e.g., unidirectionally loaded steel beam-concrete composite floors), the SCSFS achieves improved structural load-bearing efficiency and enhanced spanning capacity, making it adaptable to the requirements of larger-span buildings. The lower cable-strut system can provide reliable support for the upper rigid slab system, while the material advantages—high compressive strength of concrete and high tensile strength of cables—are fully utilized.
2) The cable-strut system adopts a spatial arrangement, which effectively restrains the lateral displacement of the lower nodes of struts, thereby ensuring the support stability of the cable-strut system.
3) The upper nodes of struts are designed to allow universal rotation, ensuring that struts only bear axial forces.
4) The cable-strut system features a simple layout with favorable visual effects; additionally, pipelines can be routed freely through the structure, resulting in high utilization efficiency of architectural space.
5) Steel beams, cables, and struts are all prefabricated components, leading to a high degree of prefabrication and accelerated construction speed.

Owing to its efficient material utilization, the Spatial Cable-Supported Floor System (SCSFS) typically features smaller component cross-sections. While this enables long spans and structural lightweighting, it also results in relatively low overall structural damping. Such characteristics—low damping, light weight, and long span—render the system prone to significant vibration responses under human-induced loads (e.g., walking, jumping, and rhythmic movements). Critically, once vibrations are excited, their attenuation process is often slow. Sustained or excessive vibrations not only severely compromise occupant comfort and disrupt normal functionality but may even trigger crowd panic or safety incidents in extreme cases. Historical and modern engineering cases—such as bridge resonance induced by specific step frequencies, severe oscillations of pedestrian bridges caused by synchronized pedestrian movements, and building-wide vibrations from fitness activities—have repeatedly demonstrated the potential risks of long-span lightweight structures under human-induced excitation [23-25].

Given the prominence of such vibration issues, major international technical standards (e.g., ISO-10137) [26] and Chinese specifications (e.g., Technical Standard for Vibration Comfort of Building Floor Structure (JGJ/T 441—2019)) [27] have provided important design guidelines and methods for human-induced vibration control. However, existing regulatory frameworks are primarily based on extensive field measurements and simplified models of traditional floor systems, such as conventional beam-slab structures, composite beams, or grid structures. As an innovative spatial tensioned cable-supported composite structure, the SCSFS exhibits unique natural vibration characteristics (frequency, mode shape) and peak acceleration responses under human-induced loads that cannot be accurately described by prediction models or limit criteria established for traditional structures. Consequently, significant doubts exist regarding the applicability and reliability of directly applying existing code provisions and evaluation methods to the human-induced vibration analysis of SCSFS. Specialized theoretical and experimental research on this novel system is therefore urgently required.

Given the pronounced human-induced vibration issues of SCSFS and the inability of existing research and specifications to directly address them, this

study systematically investigates the human-induced vibration of SCSFS through experimental and numerical simulation methods. It focuses on addressing the following key issues: (1) the natural vibration characteristics and human-induced vibration response patterns of SCSFS; (2) the influence laws of critical structural parameters on the human-induced vibration responses of SCSFS. The findings aim to provide reference for the engineering application of SCSFS.

2. Human-induced vibration testing scheme

2.1. Specimen design and fabrication

To align with the experimental setup, a spatial cable-supported floor system with a span of 4.5m × 4.5m was designed, as illustrated in Fig. 2. The outer frame employs box-shaped steel beams with a cross-section specification of □100×8 mm (height × thickness, unit: mm). Internally, H-shaped steel beams with a cross-section of H100×50×4×8 mm (height × flange width × web thickness × flange thickness, unit: mm) were used. High-strength round steel rods with a tensile strength of 650 MPa and a diameter of 20 mm serve as cables, while the struts feature a cross-section of P57×4 mm (diameter × thickness, unit: mm). The floor slab comprises 40-mm-thick reinforced concrete using C30-grade concrete. The steel beams in both longitudinal and transverse directions are connected, while the perimeter beams are welded to steel short columns at their intersections. The floor system is supported by pre-constructed concrete edge columns. Specifically, the steel short columns (Support A) are welded to embedded plates atop the concrete columns, while the steel short columns (Support B) rest directly on steel plates atop the concrete columns. Elsewhere, the bases of the steel beams are directly supported on the concrete column tops. The connections between steel short columns and cables, between cables, and between cables and struts are articulated. During construction, a 5-kN prestress was applied to the cables by rotating the cable-end tensioners. The construction process of the experimental floor system is illustrated in Fig. 3.

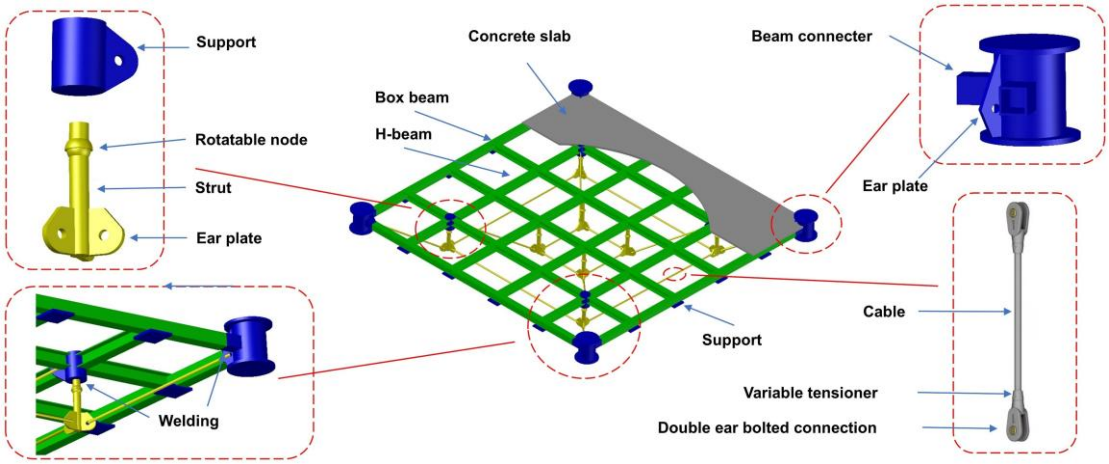

Fig. 1 Schematic diagram of the SCSFS structure

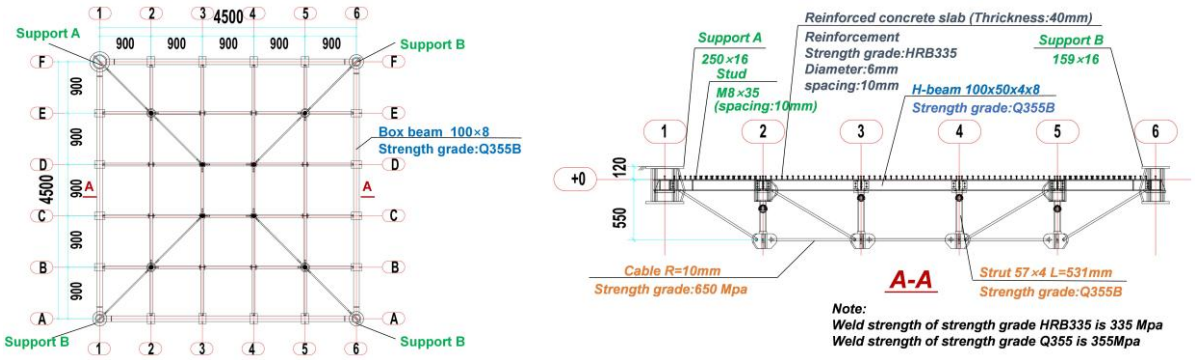

(a) Layout plan (b) Cross-sectional schematic

Fig. 2 Geometric dimensions and embedment details of the specimens (unit: mm)

(a) Steel reinforcement binding (b) Formwork removal of concrete columns and beams (c) Assembly of the steel beam grid

(d) Installation of struts and cables (e) Concrete slab construction (f) Completed floor system

Fig. 3 Construction process of the test floor

2.2. Loading scheme

Four volunteers were enlisted to apply human-induced loads to the test floor. The loading process was divided into two stages. In the first stage, a free vibration test was conducted. The volunteers applied an impact load to the test floor and then remained stationary to capture the structure's natural vibration characteristics. This stage aimed to accurately determine the natural frequency and damping ratio of the test floor.

In the second stage, the volunteers applied various types of human-induced loads, including impact, stepping, jumping, walking, and running, following predefined activity patterns. To ensure consistent excitation frequencies, a metronome was employed to regulate the volunteers' movement frequencies. This stage was designed to evaluate the human-induced vibration responses of the test floor under different load types. The volunteers' body weights are listed in Table 1, while the detailed test descriptions are provided in Table 2. The loading regions for human-induced loads are shown in Fig. 4, where A1 and A2 represent areas for impact, stepping, and jumping activities, and P1–P2 denote the walking and running paths. The loading scenarios are depicted in Fig. 5.

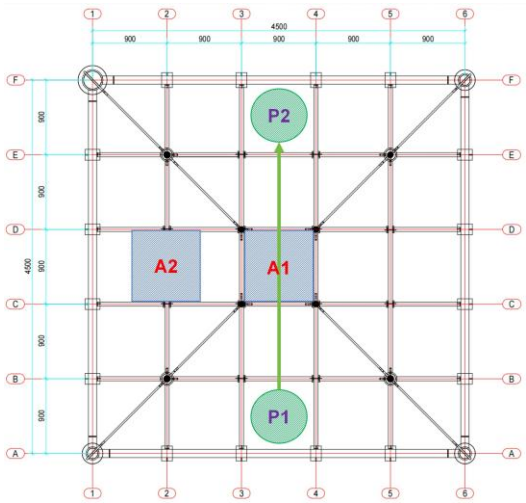

Fig. 4 Schematic diagram of the human-induced load application area

Table 1
Volunteer body weights

volunteer	1	2	3	4
weight(kg)	95	89	74	75

2.3. Measurement scheme

Since human-induced vibrations of floor systems are primarily vertical, only the vertical acceleration responses of the test floor were measured. Acceleration sensors were used at the test site to collect the vibration acceleration of the test floor, with the specific measurement scheme shown in Fig. 6. Human perception of vibration directly depends on the interaction with the contact surface, i.e., the vibration characteristics of the floor surface. Since the lower cable-strut system is not in direct contact with the human body, its vibration does not affect human perception, and thus monitoring of the lower cable-strut system is unnecessary. Moreover, considering that the vibration at the mid-span of the test floor is the most intense, acceleration sensors are arranged at the mid-span of the structure to ensure accurate capture of the maximum acceleration response of the structure.

(a) Stepping (b) Jumping

(c) Walking (d) Running

Fig. 5 On-site application of human-induced loads

3. Human-induced vibration test results and discussion

3.1. Free vibration test

The natural vibration characteristics of the test floor were determined using the results of Test 1. The heel-drop impact method was employed to obtain the free vibration acceleration decay curve, as shown in Fig. 7a. The frequency response was derived using Fast Fourier Transform (FFT), as depicted in Fig. 7b. The results indicate that the structural components exhibit typical single-periodic decay characteristics and can be modeled as a damped generalized single-degree-of-freedom system. The peak response was observed at 17.58 Hz, indicating that the first natural frequency of the test floor is 17.58 Hz. Based on the time history data, the logarithmic decrement method was applied, yielding a structural damping ratio of 0.028[28-30].

Table 2
Description of human-induced load tests

Test	description	Activity areas	Activity frequency(Hz)	Velocity (m/s)	volunteer
1	Four persons performing heel impact	A1	——	——	1、2、3、4
2	One person stepping	A1	1.89	——	2
3	Two persons stepping	A1	1.92	——	1、2
4	Three persons stepping	A1	2.00	——	1、2、4
5	Four persons stepping	A1	2.17	——	1、2、3、4
6	One person stepping	A2	1.92	——	2
7	Two persons stepping	A2	2.08	——	1、2
8	Three persons stepping	A2	2.22	——	1、2、4
9	Four persons stepping	A2	2.22	——	1、2、3、4
10	One person jumping	A1	2.33	——	2
11	Two persons jumping	A1	2.17	——	1、2
12	Three persons jumping	A1	2.00	——	1、2、4

Test	description	Activity areas	Activity frequency(Hz)	Velocity (m/s)	volunteer
13	Four persons jumping	A1	2.70	——	1、2、3、4
14	One person jumping	A2	3.03	——	2
15	Two persons jumping	A2	2.94	——	1、2
16	Three persons jumping	A2	3.03	——	1、2、4
17	Four persons jumping	A2	3.03	——	1、2、3、4
18	One person walking	P1—P2	1.66	1.33	2
19	Two persons walking	P1—P2	1.82	1.44	1、2
20	Three persons walking	P1—P2	1.50	1.00	1、2、4
21	Four persons walking	P1—P2	1.85	1.06	1、2、3、4
22	One person running	P1—P2	2.86	2.22	2
23	Two persons running	P1—P2	2.50	2.01	1、2
24	Three persons running	P1—P2	3.00	2.40	1、2、4
25	Four persons running	P1—P2	2.93	2.35	1、2、3、4

Note: The activity frequency of volunteers is calculated as "number of activity steps/time" in the experiment, and all frequencies fall within the range specified in ISO 10137 [26](1.2 – 2.4 Hz for walking, 2 – 4 Hz for running, and 1.5 – 3.5 Hz for jumping). Treading is approximately regarded as a scenario under walking.

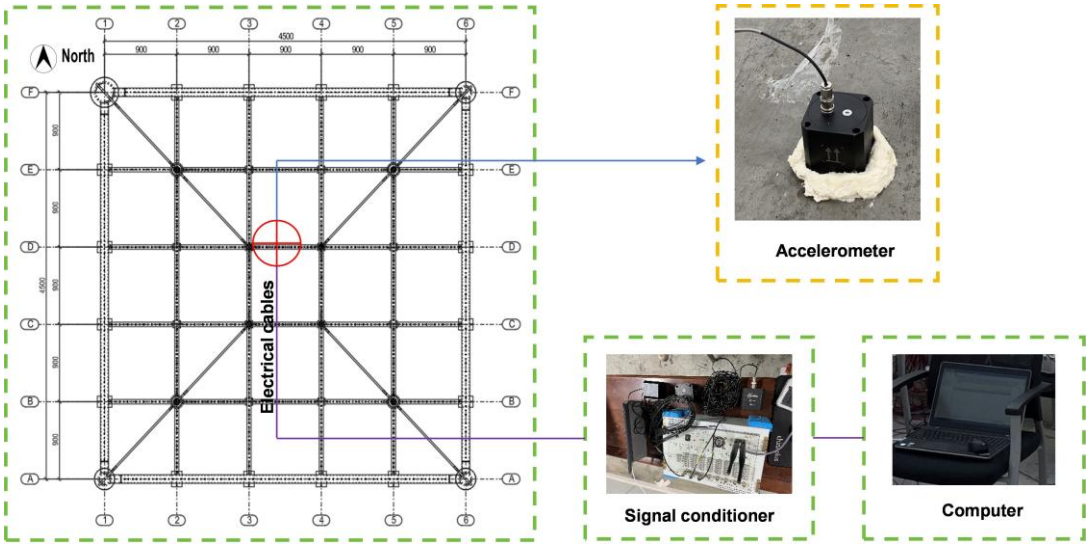

Fig. 6 Data acquisition system and typical measuring points

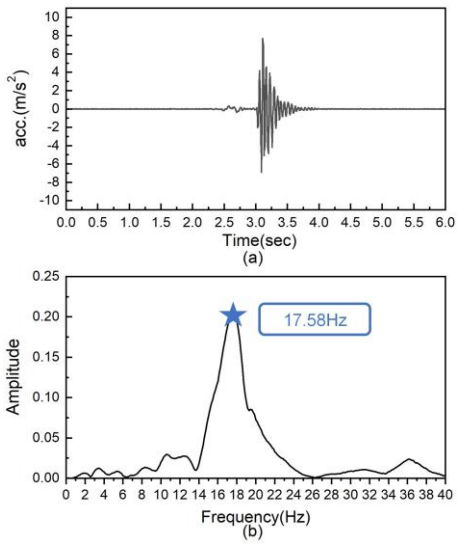

Fig. 7 Time histories and FFT results for Test 1

3.2. Human-induced vibration test

3.2.1. Stepping test

The stepping test was analyzed based on the results of Test 2. Fig. 8 illustrates that the time span between vibration peaks in the time history (i.e., the period from one peak to the next) is 0.53 seconds, corresponding to a stepping frequency of 1.89 Hz and a peak acceleration of 1.281 m/s². The FFT analysis reveals that the primary acceleration components are concentrated in the frequency ranges of 11.12–16.41 Hz and 17.22–22.51 Hz, with a peak observed at 19.34 Hz, which is ten times the stepping frequency.

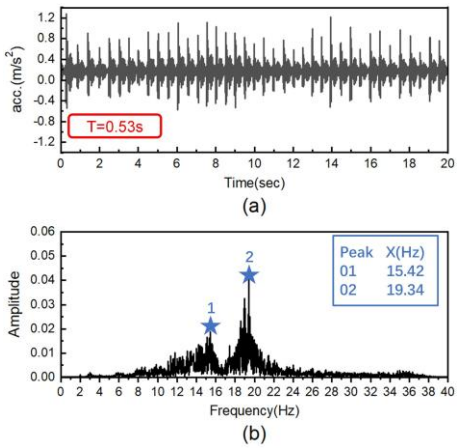

Fig. 8 Acceleration response for Test 2 (a. Time histories; b. FFT)

3.2.2. Jumping test

Due to space constraints, the jumping test was analyzed using representative results from Test 10. As shown in Fig. 9, the time history reveals a peak period

of 0.43 seconds, corresponding to a jumping frequency of 2.33 Hz and a peak acceleration of 1.121 m/s². The FFT analysis indicates primary acceleration components at 2.36 Hz, 4.65 Hz, 7.05 Hz, 9.41 Hz, 11.81 Hz, 13.84 Hz, and within the range of 16.83–19.95 Hz, with a peak observed at 18.75 Hz, which is eight times the jumping frequency.

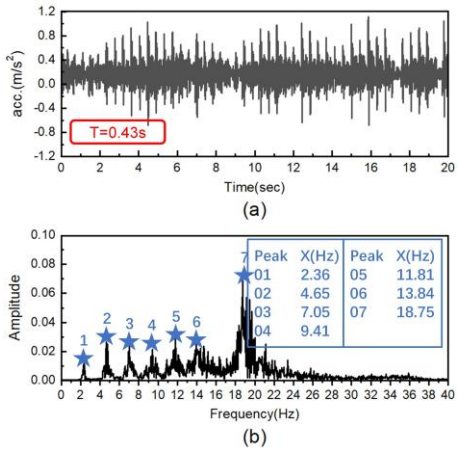

Fig. 9 Acceleration response for Test 10 (a. Time histories; b. FFT)

3.2.3. Walking test

The walking test was analyzed based on representative results from Test 21. Fig. 10 shows a peak period of 0.54 seconds, corresponding to a walking frequency of 1.85 Hz and a peak acceleration of 1.173 m/s². The FFT results show a peak at 18.55 Hz, which is ten times the walking frequency.

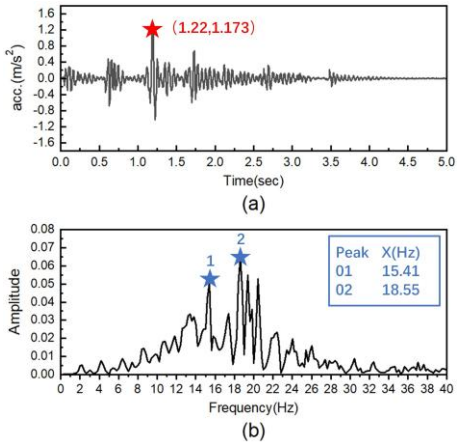

Fig. 10 Acceleration response for Test 21 (a. Time histories; b. FFT)

3.2.4. Running test

The running test was analyzed using the results of Test 22. Fig. 11 shows a time history peak period of 0.35 seconds, corresponding to a running frequency of 2.86 Hz and a peak acceleration of 0.996 m/s². The FFT analysis indicates primary acceleration components within the ranges of 2.00–3.83 Hz and 8.05–24.26 Hz, with a peak observed at 19.67 Hz, which is seven times the running frequency.

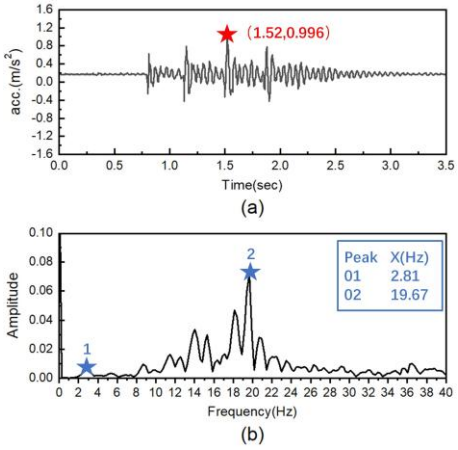

Fig. 11 Acceleration response for Test 22 (a. Time histories; b. FFT)

3.2.5. Summary and discussion of human-induced vibration responses

The peak acceleration responses across all test cases are summarized in Table 3. The results indicate that the peak accelerations of Tests 2–5 are greater than those of Tests 6–9, while the peak accelerations of Tests 10–13 exceed those of Tests 14–17. Since the acceleration sensors are arranged in the mid-span region, when excitation is applied at the mid-span, the floor vibration is dominated by the first-order mode shape, with the mid-span being the area of maximum vibration response. Additionally, the excitation positions in Tests 10–13 are closer to the sensors (see Table 2 for details), resulting in higher acceleration signals. The peak accelerations under jumping loads in Tests 10–13 are significantly higher than those induced by other types of loads. Tests 18–21 correspond to peak accelerations under walking loads, which are relatively small.

In accordance with the Technical Standard for Vibration Comfort of Building Floor Structure [27], the peak accelerations of Tests 2–25 all exceed the specified peak acceleration limits, indicating that the test floor has significant issues regarding human-induced vibrations.

Table 3
Summary of peak responses to human-induced vibration

stepping		jumping		walking		running	
test number	peak acceleration(m/s²)	test number	peak acceleration(m/s²)	test number	peak acceleration(m/s²)	test number	peak acceleration(m/s²)
2	1.281	10	1.121	18	0.46	22	0.996
3	0.973	11	5.852	19	0.281	23	0.868
4	1.275	12	4.86	20	0.962	24	1.231
5	1.633	13	4.412	21	1.173	25	0.978
6	0.516	14	1.301	——	——	——	——
7	0.613	15	1.497	——	——	——	——
8	1.275	16	3.135	——	——	——	——
9	1.497	17	2.716	——	——	——	——

4. Finite element analysis

4.1. Modeling scheme

The finite element model of the Test floor was developed using the ABAQUS software, as illustrated in Fig. 12. The steel beams beneath the slab were modeled using beam elements (B31), with Young's modulus, density, and Poisson's ratio (PRXY) defined as 2.06e11 N/mm², 7850 kg/m³, and 0.3, respectively. The concrete slab was modeled using shell elements (S4R), with corresponding values of 3e10 N/mm², 2400 kg/m³, and 0.2. Truss elements (T3D2) were employed to simulate the struts and cables beneath the slab, sharing the same material properties as the steel beams. The boundary conditions were

set to align with the experimental setup, where one corner of the floor system (RP-1) was restrained in all three translational directions, while the other three corners and steel beam supports (RP-2) were constrained in the vertical direction only.

The load point (LP1) corresponded to the location of jumping and stepping loads, while single-running loads were applied along route LR1, and four-person walking loads were applied along route LR2. The magnitude and frequency of the loads were consistent with those in the experiment, and the acceleration response was measured at the same location as the applied load (LP1). Table 5 summarizes the parameters of the finite element model.

Human-induced loads were simulated using the Fourier series model specified in ISO 10137 [26], as expressed in Equation (1):

$$F_v(t) = Q\left[1 + \sum_{n=1}^{k} \alpha_{n,v} \sin\left(2\pi n f t + \phi_{n,v}\right)\right] \quad (1)$$

In the equation, Q represents the individual weight (N), n is the harmonic order, k is the number of harmonics, $\alpha_{n,v}$ is the Fourier coefficient for the nth harmonic, f is the step frequency, and $\phi_{n,v}$ is the phase of the nth harmonic (rad). Parameters of the load model are determined based on Table 4. To enable effective comparison between finite element analysis results and on-site measured data, the fundamental frequency adopts the actual excitation frequencies obtained from on-site measurement statistics. The moving load is applied in the following manner: the position of the load action is dynamically adjusted along the longitudinal direction of the floor system. When a load is applied at a new position, the load at the previous position is removed simultaneously. The step distance is set to 720 mm, and the time interval for position switching is equal to the step frequency. Moreover, at each action position, a complete time history curve of single-step walking force is applied to simulate the moving effect of real walking loads.

Table 4
Parameter values of human-induced load model

Type of Motion	Frequency (Hz)	First Three Fourier Coefficients		
		α_1	α_2	α_3
Stepping	1.89	0.33	0.1	0.06
Jumping	2.33	1.40	0.4	0.10
	2.50	1.40	0.4	0.10
Walking	1.85	0.31	0.1	0.06
Running	2.86	1.40	0.4	0.10
	2.50	1.40	0.4	0.10

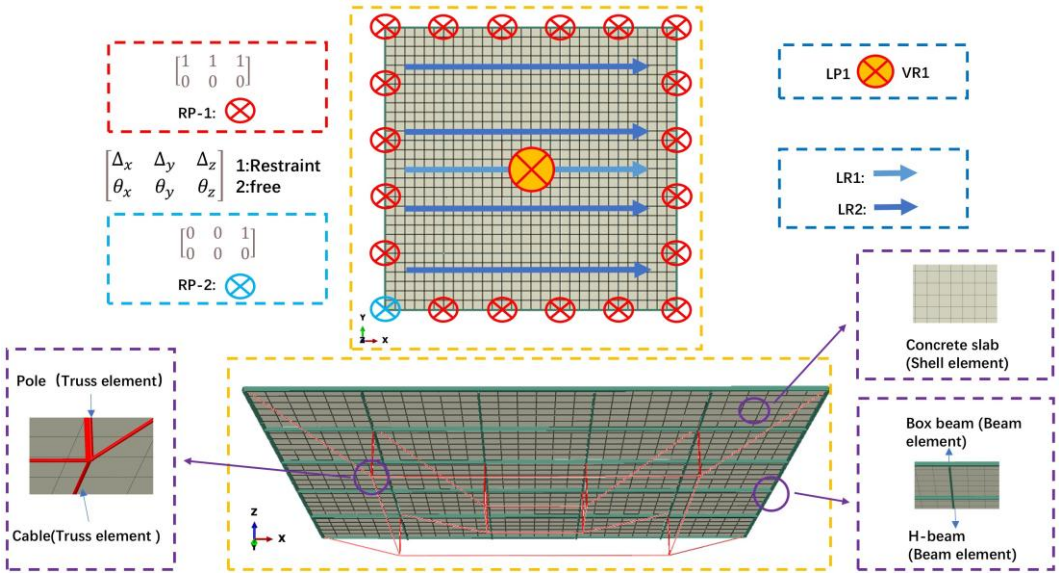

Fig. 12 Finite element model of the test floor

Table 5
Description of finite element model parameters

Model Number	Parameter Information										
	Floor Area (mm^2)	Sag (mm)	Slab Thickness (mm)	Beam Height (mm)	Beam Section Type	Cable Cross-sectional Area (mm^2)	Strut Cross-sectional Area (mm^2)	Cable Prestress (KN)	Inner Cables	Outer Cables	Boundary condition
Test floor	4500*4500	1293	50	100	H	314	1381	5	√	√	A
SCSFS-1	13500*13500	1293	50	100	H	314	1381	5	√	√	A
SCSFS-2	13500*13500	1293	50	100	H	314	1381	5	×	×	A
SCSFS-3	13500*13500	1293	50	100	H	314	1381	5	×	√	A
SCSFS-4	13500*13500	1293	50	100	H	314	1381	5	√	×	A
SCSFS-5	13500*13500	1293	50	100	box	314	1381	5	√	√	A
SCSFS-6	13500*13500	1293	60	100	H	314	1381	5	√	√	A
SCSFS-7	13500*13500	1293	70	100	H	314	1381	5	√	√	A
SCSFS-8	13500*13500	1293	80	100	H	314	1381	5	√	√	A
SCSFS-9	13500*13500	1293	90	100	H	314	1381	5	√	√	A
SCSFS-10	13500*13500	1293	100	100	H	314	1381	5	√	√	A
SCSFS-11	13500*13500	1293	50	125	H	314	1381	5	√	√	A
SCSFS-12	13500*13500	1293	50	150	H	314	1381	5	√	√	A

SCSFS-13	13500*13500	1293	50	175	H	314	1381	5	√	√	A
SCSFS-14	13500*13500	1293	50	200	H	314	1381	5	√	√	A
SCSFS-15	13500*13500	1293	50	100	H	392.5	1381	5	√	√	A
SCSFS-16	13500*13500	1293	50	100	H	471	1381	5	√	√	A
SCSFS-17	13500*13500	1293	50	100	H	549.5	1381	5	√	√	A
SCSFS-18	13500*13500	1293	50	100	H	628	1381	5	√	√	A
SCSFS-19	13500*13500	1293	50	100	H	314	1727	5	√	√	A
SCSFS-20	13500*13500	1293	50	100	H	314	2072	5	√	√	A
SCSFS-21	13500*13500	1293	50	100	H	314	2417.8	5	√	√	A
SCSFS-22	13500*13500	1293	50	100	H	314	2763.2	5	√	√	A
SCSFS-23	13500*13500	1293	50	100	H	314	1381	5	√	√	B
SCSFS-24	13500*13500	1293	50	100	H	314	1381	5	√	√	C
SCSFS-25	13500*13500	1293	50	100	H	314	1381	5	√	√	D
SCSFS-26	13500*13500	1293	50	100	H	314	1381	10	√	√	A
SCSFS-27	13500*13500	1293	50	100	H	314	1381	15	√	√	A
SCSFS-28	13500*13500	1293	50	100	H	314	1381	20	√	√	A
SCSFS-29	13500*13500	906	50	100	H	314	1381	5	√	√	A
SCSFS-30	13500*13500	1035	50	100	H	314	1381	5	√	√	A
SCSFS-31	13500*13500	1164	50	100	H	314	1381	5	√	√	A
SCSFS-32	13500*13500	1422	50	100	H	314	1381	5	√	√	A
SCSFS-33	13500*13500	1293	120	250	H	900	1381	5	√	√	A
SCSFS-34	13500*13500	1164	140	250	H	900	1381	5	√	√	A
SCSFS-35	13500*13500	1422	260	300	H	1500	1381	5	√	√	A

Note: Boundary condition A—corner three-way translational constraints, the rest only constraints vertical translational constraints; Boundary condition B—All use three-way translation constraints; Boundary condition C—Release the tangential translational constraints of the floor system and apply only the translational constraints in the other two directions; Boundary condition D—releases the normal translational constraints of the floor system and applies only the translational constraints in the other two directions.

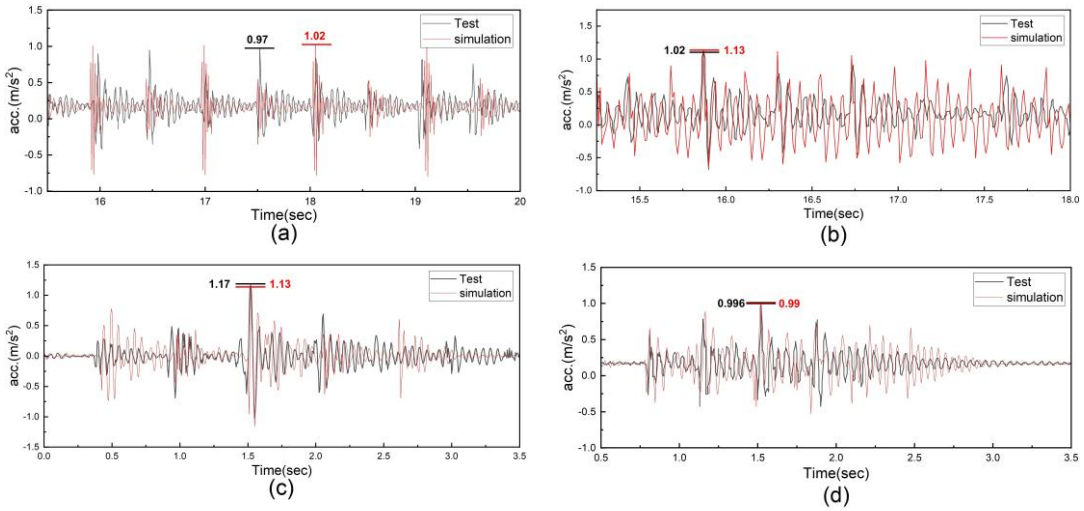

Fig. 13 Comparison of simulated and measured dynamic responses of the floor system (a. Dynamic response under single-person stepping load; b. Dynamic response under single-person jumping load; c. Dynamic response under four-person walking load; d. Dynamic response under single-person running load).

Table 6
Numerical simulation results of natural characteristics for SCSFS-1

Mode Shape Number	1	2	3
Frequency (Hz)	2.68	2.89	4.45
Mode Shape	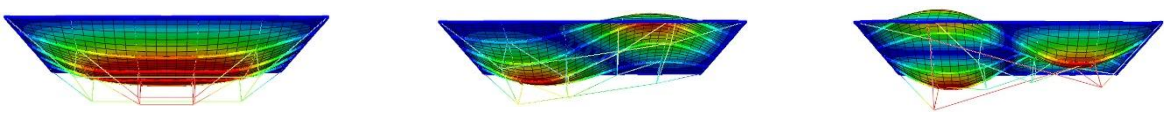		

4.2. Validation of the modeling scheme

Based on the aforementioned finite element model (TEST FLOOR), a finite element analysis was conducted, and the results were compared with the experimental data. In terms of natural frequency, the first-order frequency obtained from the finite element analysis was 18.11 Hz, while the first-order

natural frequency measured in the experiment was 17.58 Hz, with an error of 3%. According to relevant studies [31-33], an error of 3% is acceptable.

Fig. 13 presents the comparison of human-induced vibration responses obtained from experiments and FEA. Under single-person stepping, single-person jumping, four-person walking, and single-person running loads, the peak accelerations obtained from the numerical simulations were 1.02 m/s², 1.13 m/s²,1.13 m/s², and 0.99 m/s², respectively, while the experimentally measured peak accelerations were 0.97 m/s², 1.02 m/s², 1.17 m/s², and 0.996 m/s², respectively. The errors between the numerical simulations and the experimentally measured peak accelerations were 5%, 10%, 3%, and 1%, respectively. The 10% error corresponding to the jumping load is mainly attributed to the fact that the finite element analysis adopts the standard load model specified in the ISO 10137 [26] standard. However, in the actual test, there are significant individual differences among volunteers in terms of jumping movements, jumping heights, and motor abilities, resulting in deviations between the actual load and the standard model in the specification, which in turn leads to this error.

In summary, the numerical simulations were able to accurately reflect the dynamic response characteristics of the floor system under various loads. Although minor errors were present, the overall trends and peak patterns were consistent, validating the reliability of the adopted modeling approach in predicting the dynamic response of the floor system.

4.3. Human-induced vibration of SCSFS-1

Given that the test floor was subsequently scheduled for static load tests, larger cross-sectional dimensions were designed for safety considerations. This resulted in increased stiffness and a higher natural frequency, which deviated from the typical frequency range of human-induced loads (1.5 Hz–3.5 Hz). To further investigate the vibration response mechanism of the floor under such loads while maintaining the structural configuration unchanged, a validated finite element scheme was employed to establish a floor model with a span exceeding 10 m. This model not only embodies the characteristics of large-span floors but also brings the floor's frequency closer to the excitation frequency of human activities, thereby more comprehensively revealing the vibration characteristics of the floor under human-induced loads. The key parameters of the adjusted model (SCSFS-1) are listed in Table 5.

Load application areas and acceleration measurement points are shown in Fig. 12. LP1 denotes the application point for jumping and stepping loads, while LR1 and VR1 represent the routes and central point for running and walking loads. The load excitation time histories were calculated using Equation (1), in which the individual weight Q was taken as 0.882kN and the excitation frequency f was set to 2.5 Hz.

4.3.1. Natural vibration characteristics

The natural vibration characteristics of the modified finite element model were analyzed, as summarized in Table 6. The first-order natural frequency of SCSFS-1 was 2.68 Hz, corresponding to a half-wave mode. The second-order natural frequency was 2.89 Hz, with two half-wave modes, while the third-order frequency was 4.45 Hz, featuring four half-wave modes.

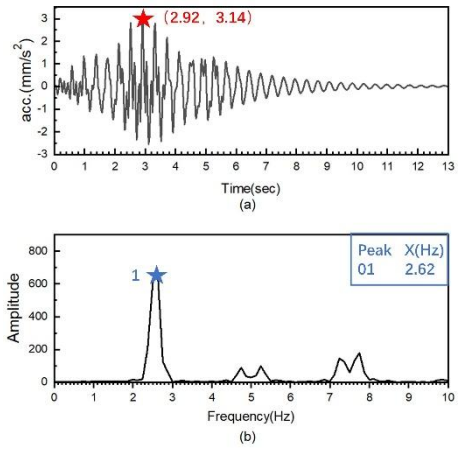

Fig. 14 Time histories and FFT results of SCSFS-1 under running load

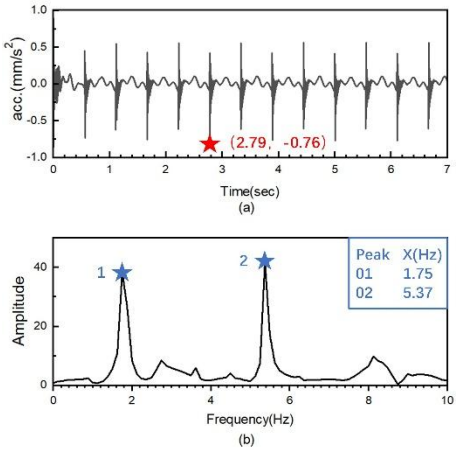

Fig. 15 Time histories and FFT results of SCSFS-1 under stepping load

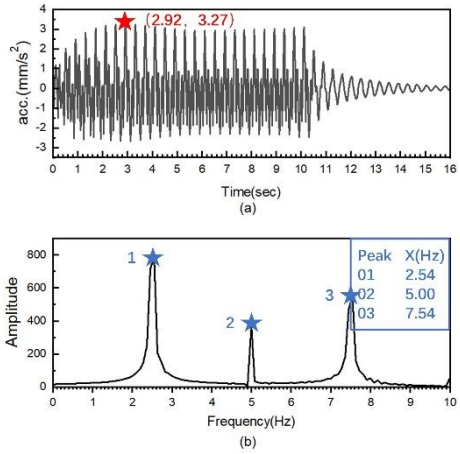

Fig. 16 Time histories and FFT results of SCSFS-1 under jumping load

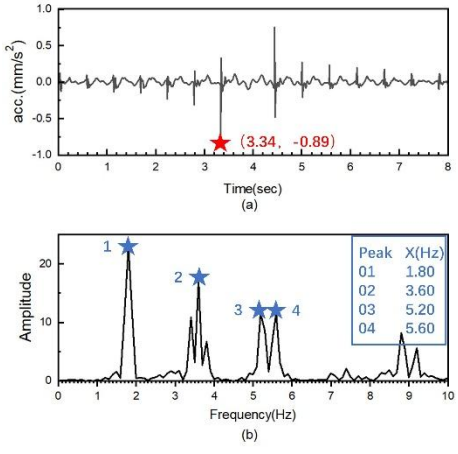

Fig. 17 Time histories and FFT results of SCSFS-1 under walking load

4.3.2. Human-induced vibration response

Under running loads (Fig. 14), the peak acceleration was 3.14 m/s², with dominant FFT components observed in the ranges of 2.2–3.0 Hz, 4.5–5.5 Hz, and 7–8 Hz. A peak occurred at 2.62 Hz, primarily exciting the first-order mode (2.68 Hz).

For stepping loads (Fig. 15), the peak acceleration was 0.76 m/s², with FFT components concentrated in the ranges of 1.0–2.2 Hz and 5.1–6.4 Hz. A peak was observed at 5.37 Hz.

Under jumping loads (Fig. 16), the peak acceleration reached 3.27 m/s², with FFT components in the ranges of 2–3 Hz, 4.8–5.2 Hz, and 7–8 Hz. A peak at 2.54 Hz primarily excited the first-order mode.

Finally, for walking loads (Fig. 17), the peak acceleration was 0.89 m/s², with FFT components appearing in the ranges of 1.6–2.0 Hz, 3.2–4.0 Hz, 4.8–6.0 Hz, and 8.2–9.8 Hz. A peak at 1.8 Hz was observed.

4.4. Parametric analysis

Key parameters of the floor system, including the arrangement of cable-

strut system, slab thickness, steel beam section type, beam height, cable cross-sectional area, strut cross-sectional area, boundary conditions, cable prestress, and sag of cable-strut system, were selected to investigate their influence on the human-induced vibration responses of the floor system. The model parameters are listed in Table 5. Given that the human-induced vibration responses of the floor system are most significant under jumping and running loads, these two load types were applied as excitations during the parametric analysis.

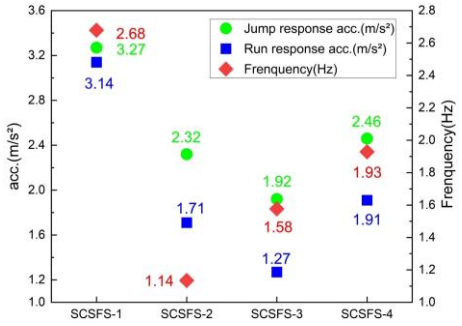

Fig. 18 Natural frequency and peak acceleration under different arrangements of cable-strut system

4.4.1. Arrangement of cable-strut system

Fig. 18 illustrates the effects of four different arrangements of cable-strut system configurations on the floor system's natural frequency and peak acceleration under jumping and running loads.

In terms of natural vibration characteristics, using the natural frequency of SCSFS-1 (2.68 Hz) as the baseline, the frequency changes for SCSFS-2, SCSFS-3, and SCSFS-4 were -57.5%, -41.0%, and -30.0%, respectively.

In terms of human-induced vibration response under running load, using the acceleration response of SCSFS-1 (3.14 m/s²) as the baseline, the changes in acceleration response for SCSFS-2, SCSFS-3, and SCSFS-4 were -45.5%, -59.6%, and -39.2%, respectively. Under jumping load, using the acceleration response of SCSFS-1 (3.27 m/s²) as the baseline, the changes in acceleration response for SCSFS-2, SCSFS-3, and SCSFS-4 were -29.1%, -41.3%, and -24.8%, respectively.

These data indicate that the inner-ring cables contribute significantly more to enhancing the floor system's stiffness than the outer-ring cables. Specifically, the outer-ring cables reduce the acceleration response, whereas the inner-ring cables lead to an increase in the acceleration response. This phenomenon stems from the fact that the structural vibration response is determined by the combined action of multiple factors, such as mass, stiffness, load type, and load frequency, rather than being solely dependent on stiffness. Meanwhile, the actual vibration of the floor system is dominated by the superposition of multiple modes rather than a single mode. When the inner-ring cables significantly increase the structural stiffness, elevating the structural frequency to a level close to or even consistent with the excitation frequency of human-induced loads, resonance effects may be triggered, thereby amplifying the human-induced vibration response of the structure.

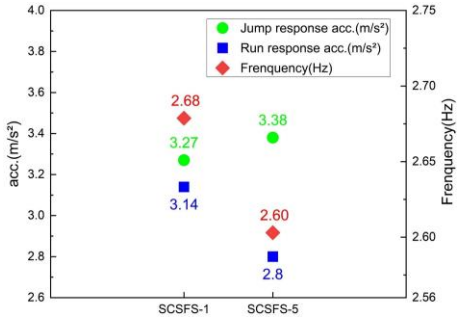

Fig. 19 Natural frequency and peak acceleration under different steel beam cross-section types

4.4.2. Steel beam section type

Fig. 19 illustrates the effects of the steel beam section type on the floor system's natural frequency and peak acceleration under jumping and running loads.

In terms of natural vibration characteristics, the natural frequency of SCSFS-1 was 2.68 Hz, which was approximately 2.9% higher than that of SCSFS-5 (2.60 Hz). This difference was primarily attributed to the increase in mass, which partially offset the enhancement in stiffness.

In terms of human-induced vibration response under running load, the acceleration response of SCSFS-1 was 3.14 m/s², which was significantly higher than that of SCSFS-5 (2.80 m/s²), with a difference of approximately 12.14%. Under jumping load, the acceleration response of SCSFS-1 was 3.27 m/s², which was lower than that of SCSFS-5 (3.38 m/s²), with a difference of approximately 3.36%.

These data indicate that the steel beam section type not only influences the natural frequency of the floor system but also affects the acceleration response, with distinct response trends observed under different load types.

4.4.3. Slab thickness

Fig. 20 demonstrates the effects of varying slab thickness on the floor system's natural frequency and peak acceleration under jumping and running loads.

In terms of natural vibration characteristics, using the natural frequency of SCSFS-1 (2.68 Hz) as the baseline, the frequency changes for SCSFS-6, SCSFS-7, SCSFS-8, SCSFS-9, and SCSFS-10 were -2.6%, -3.4%, -3.0%, -1.9%, and 0%, respectively.

In terms of human-induced vibration response under running load, using the acceleration response of SCSFS-1 (3.14 m/s²) as the baseline, the changes in acceleration response for SCSFS-6, SCSFS-7, SCSFS-8, SCSFS-9, and SCSFS-10 were -32.5%, -38.5%, -45.2%, -55.1%, and -64.6%, respectively. Under jumping load, using the acceleration response of SCSFS-1 (3.27 m/s²) as the baseline, the changes in acceleration response for SCSFS-6, SCSFS-7, SCSFS-8, SCSFS-9, and SCSFS-10 were -21.4%, -34.9%, -43.7%, -54.4%, and -63.6%, respectively.

These data indicate that an increase in slab thickness initially reduces the natural frequency of the floor system, followed by an increase, while the acceleration response gradually decreases.

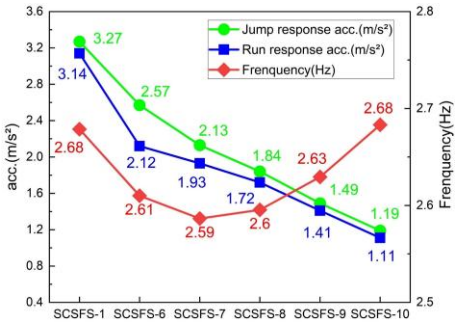

Fig. 20 Natural frequency and peak acceleration under different slab thicknesses

4.4.4. Beam height

Fig. 21 presents the effects of varying beam height on the floor system's natural frequency and peak acceleration under jumping and running loads.

In terms of natural vibration characteristics, when the beam height was increased from 100 mm (SCSFS-1) to 200 mm (SCSFS-14), the natural frequency was increased by 19%.

In terms of human-induced vibration response under running load, as the beam height was increased from 100 mm to 200 mm, the acceleration response of the floor system exhibited a significant decreasing trend, with a total reduction of 79%. Under jumping load, when the beam height was increased from 100 mm to 200 mm, the acceleration response of the floor system also demonstrated a gradual decreasing trend, with an overall reduction of 63%.

These data indicate that an increase in beam height leads to a gradual rise in the natural frequency of the floor system, while the acceleration response progressively decreases.

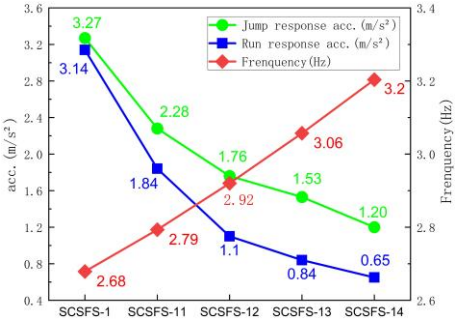

Fig. 21 Natural frequency and peak acceleration under different beam heights

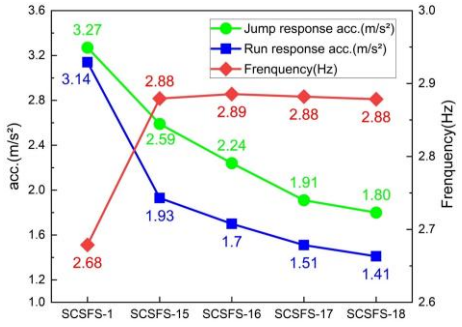

Fig. 22 Natural frequency and peak acceleration under different cable cross-sectional areas

4.4.5. Cable cross-sectional area

Fig. 22 illustrates the influence of varying cable cross-sectional areas on the natural frequency of the floor system and its peak acceleration under jumping and running loads.

In terms of natural vibration characteristics, when the cable cross-sectional area was increased from 314 mm² (SCSFS-1) to 392.5 mm² (SCSFS-15), the natural frequency was increased by approximately 7.5%, and the first-order vibration mode of the floor system transitioned from one half-wave to two half-waves. When the cable cross-sectional area was further increased from 392.5 mm² to 628 mm² (SCSFS-18), the natural frequency remained almost unchanged. This phenomenon was attributed to the fact that the first-order vibration mode of the floor system had already transitioned to two half-waves, at which point the change in cable cross-sectional area had a relatively minor influence.

In terms of human-induced vibration response under running load, as the cable cross-sectional area was increased from 314 mm² to 628 mm², the acceleration response exhibited a decreasing trend, with a total reduction of 55.1%. Under jumping load, when the cable cross-sectional area was increased from 314 mm² to 628 mm², the acceleration response gradually decreased, with a total reduction of 45.0%.

These data indicate that increasing the cable cross-sectional area can significantly reduce the acceleration response and enhance the natural frequency of the floor system, although it may lead to changes in the vibration mode shapes of the floor system.

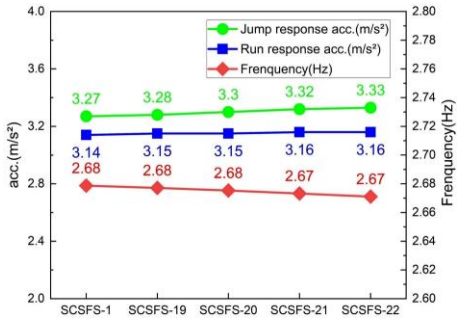

Fig. 23 Natural frequency and peak acceleration under different strut cross-sectional areas

4.4.6. Strut cross-sectional area

Fig. 23 depicts the impact of varying strut cross-sectional areas on the natural frequency of the floor system and its peak acceleration under jumping and running loads.

In terms of natural vibration characteristics, the increase in strut cross-sectional area had a limited influence on the natural frequency, with a variation not exceeding 0.02 Hz. In terms of human-induced vibration response, the variation in acceleration response did not exceed 0.06 m/s². These data indicate that changes in strut cross-sectional area have a minor influence on both the natural frequency and acceleration response of the floor system.

4.4.7. Floor system boundary condition

Fig. 24 illustrates the influence of different boundary conditions on the natural frequency of the floor system and its peak acceleration under jumping and running loads.

Under different constraint conditions, the variation range of the natural vibration frequency is extremely limited, not exceeding 0.02 Hz, and the variation is less than 1%. Under the action of running and jumping loads, the variation range of the acceleration response of each model is also small, with a variation of less than 1%. These data indicate that the boundary conditions of the floor have a relatively small impact on the natural vibration frequency and acceleration response of the floor.

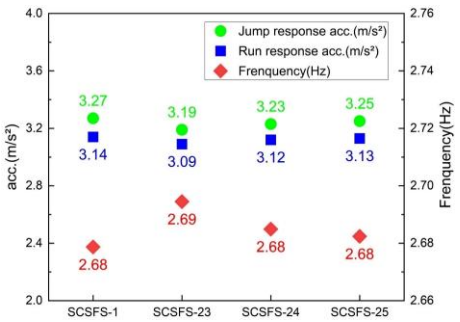

Fig. 24 Natural frequency and peak acceleration under different floor system boundary conditions

4.4.8. Cable prestress

Fig. 25 illustrates the effect of varying cable prestress on the natural frequency and peak acceleration of the floor system under jumping and running loads.

The research results show that under the prestress conditions of 5kN, 10kN, 15kN, and 20kN, the natural frequency of the floor system remains unchanged, and the peak acceleration remains basically consistent. This is attributed to the fact that the boundary conditions of the floor system fully release the horizontal constraints, causing the prestress of the cables to be entirely borne and compressed by the upper rigid structure. A self-balancing state is formed between the "improvement of geometric stiffness" by the cables and the "reduction of geometric stiffness due to compression" of the upper structure. The influences of the two on the geometric stiffness offset each other, so the prestress has no significant impact on the overall dynamic response.

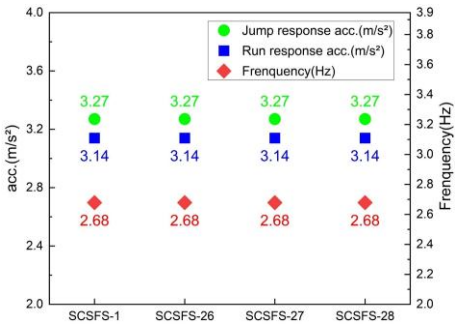

Fig. 25 Natural frequency and peak acceleration under different cable prestress levels

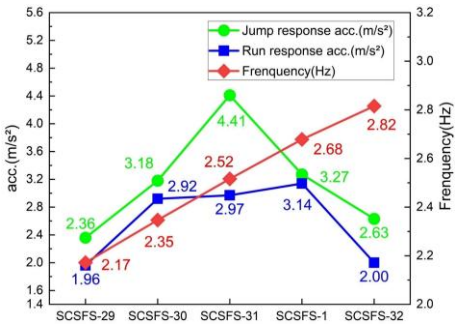

Fig. 26 Natural frequency and peak acceleration under different sags

4.4.9. Sag of cable-strut system

Fig. 26 illustrates the influence of different sags (where sag refers to the vertical distance along the vertical direction between the two ends of the cable) on the natural frequency of the floor system and its peak acceleration under jumping and running loads.

In terms of natural vibration characteristics, when the sag was increased from 906 mm (SCSFS-29) to 1422 mm (SCSFS-32), the natural frequency was increased by approximately 30%.

In terms of human-induced vibration response under running load, using the acceleration response of SCSFS-29 (1.96 m/s²) as the baseline, the changes in acceleration response for SCSFS-30, SCSFS-31, SCSFS-1, and SCSFS-32

were 49.0%, 51.5%, 60.2%, and 2.0%, respectively. Under jumping load, using the acceleration response of SCSFS-29 (2.36 m/s²) as the baseline, the changes in acceleration response for SCSFS-30, SCSFS-31, SCSFS-1, and SCSFS-32 were 34.7%, 86.9%, 38.6%, and 11.4%, respectively.

These data indicate that as the sag increases, the natural frequency of the floor system gradually rises, while the acceleration response exhibits a trend of initial increase followed by a decrease.

4.5. Vibration control schemes based on comfort limit requirements

Fig. 27 presents the models that meet the comfort limit requirements. By adjusting the sag, slab thickness, and beam height, the peak acceleration of the floor system has been reduced. The same excitation method as used in the parameter influence analysis in Section 4.4 was adopted herein.

In accordance with the Technical Standard for Vibration Comfort of Building Floor Structure [27], SCSFS-33, SCSFS-34, and SCSFS-35 satisfy the limit requirements for such spaces as dance halls, performance stages, spectator stands, indoor sports venues, and gyms dedicated to aerobic exercises. Specifically, during normal use, the first-order vertical natural frequency of the floor system should not be less than 4 Hz, and the effective maximum vertical vibration acceleration should not exceed 0.5 m/s².

SCSFS-35 meets the requirements for spaces including shopping malls, restaurants, public transportation waiting halls, theaters, cinemas, auditoriums, and exhibition halls. For these venues, the first-order vertical natural frequency of the floor system should not be less than 3 Hz, and the peak vertical vibration acceleration should not exceed 0.15 m/s².

4.6. Comparative analysis of natural vibration characteristics of typical floor systems

To clarify the differences among the spatial cable-supported floor system (SCSFS-1), steel-concrete composite floor system (SCSFS-2), and steel truss composite floor system, a comparative group was established through numerical simulation. Specifically, based on SCSFS-1, two comparative models were constructed: one is SCSFS-2 with cables and struts removed, and the other is a steel truss composite floor system where cables and struts are replaced by steel trusses with the same material consumption maintained. The relevant comparison results are presented in Table 7.

The natural vibration frequency of the SCSFS-1 system is 2.68 Hz. Although it is lower than 3.29 Hz of the steel truss composite floor system, it is significantly higher than 1.14 Hz of the steel-concrete composite floor system (SCSFS-2). This indicates that the presence of cables can enhance the floor stiffness, optimize the vibration characteristics of the floor to a certain extent, and reduce the risk of comfort problems caused by human-induced vibration.

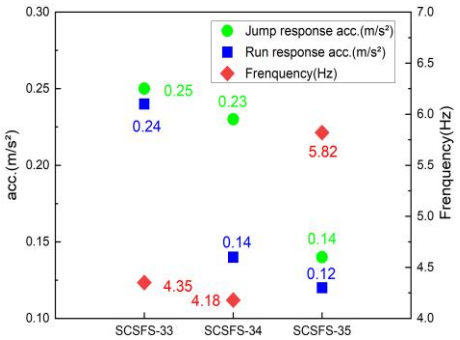

Fig. 27 Vibration response indices of SCSFS models meeting comfort requirements for different venues

Table 7
Numerical simulation comparison of natural vibration characteristics of three typical floor systems

Name	SCSFS - 1	Steel - Concrete Composite Floor (SCSFS - 2)	Steel Truss Composite Floor
First - order Natural Vibration Frequency (Hz)	2.68	1.14	3.29
Mode Shape	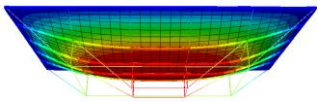	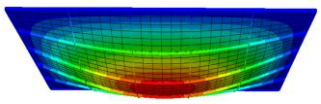	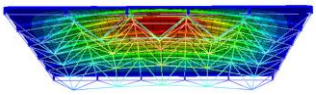

Note: The steel-concrete composite floor (SCSFS-2) is developed from SCSFS-1 by removing the cables and struts; the steel truss composite floor is developed from SCSFS-1 by replacing the cables and struts with steel trusses, ensuring that the material consumption of SCSFS-1 is consistent with that of the steel truss composite floor.

5. Conclusions

This study systematically investigated the dynamic response of the spatial cable-supported floor system under various human-induced loads through on-site experiments and numerical simulations, with a focus on the natural vibration characteristics, human-induced vibration responses, and the impact of key structural parameters on vibration behavior. The experimental loading included free vibration tests and multiple human-induced vibration tests, covering four common excitation types: stepping, jumping, walking, and running. The main findings are as follows:

1) The test floor exhibited a first-order natural frequency of 17.58 Hz and a damping ratio of 0.028. Significant vibration issues were observed under human-induced loads, with jumping loads having the most pronounced effect on acceleration response, resulting in a maximum peak response of 5.852 m/s². In contrast, walking loads produced minimal effects on acceleration response.
2) The cross-sectional type of steel beams influenced not only the natural frequency of the floor system but also its acceleration response. Different load types resulted in varying response trends. Increasing the slab thickness initially reduced the natural frequency of the floor system but subsequently led to an increase, while acceleration responses progressively decreased. Conversely, increasing the beam height consistently elevated the natural frequency and concurrently reduced the acceleration response.
3) The cable-strut system significantly improved the natural frequency of the floor system. The inner-ring cables contributed more to stiffness enhancement than the outer-ring cables. Both inner- and outer-ring cables affected the acceleration response of the floor system: outer-ring cables reduced acceleration responses, whereas inner-ring cables increased them. Increasing the cable cross-sectional area markedly reduced acceleration responses and improved the natural frequency of the floor system, although it could alter the vibration mode shapes. The presence or absence of cable prestress had no observable effect on the natural frequency or acceleration responses of the floor system.
4) The cross-sectional area of struts and the boundary conditions of the floor system had minimal influence on the natural frequency and acceleration responses. With increasing sag, the natural frequency of the floor system gradually increased, while acceleration responses exhibited a trend of initial increase followed by a decrease.
5) It is possible to reduce the vibration response of the floor and increase its natural vibration frequency by optimizing the key structural parameters of the floor (multi - parameter coordination), so that all indicators meet the comfort limit requirements of the Technical Standard for Vibration Comfort of Building Floor Structures [27], providing a quantifiable engineering solution for floor vibration control.

Acknowledgements

The project received financial support from the Shandong Provincial Natural Science Foundation, China (Grant No. ZR2020QE243).

References

[1] Bazli M, Heitzmann M, Ashrafi H, "Long-span timber flooring systems: A systematic review

from structural performance and design considerations to constructability and sustainability aspects", Journal of Building Engineering, 48, 103981, 2022.
[2] Zhang X, Li Q, Wang Y, et al., "Numerical and Experimental Study on the Dynamic Behavior of an Innovative Steel-Concrete Composite Hollow Waffle Floor", International Journal of Structural Stability & Dynamics, 20(8), 0, 2020.
[3] Choe L, et al., "Behavior and Limit States of Long-Span Composite Floor Beams with Simple Shear Connections Subject to Compartment Fires: Experimental Evaluation", Journal of Structural Engineering, 146(6), 1 – 14, 2020.
[4] Tan M, Wu Y, Pan W, et al., "Optimal Design of a Novel Large-Span Cable-Supported Steel – Concrete Composite Floor System", Buildings, 14(1), 113, 2024.
[5] Zhou L, Huang Y, Chen B, et al., "Seismic Behavior of Large-Span Open-Web Floors Consisting of I-Shaped Steel Chords and Steel Tube Webs", Advances in Civil Engineering, 2020, 1 – 14, 2020.
[6] Cao L, Li J, Zheng X, Chen Y F, "Vibration behavior of large span composite steel bar truss-reinforced concrete floor due to human activity", Steel and Composite Structures, An International Journal, 37(4), 391 – 404, 2020.
[7] Yang S, Wang G, Xu Q, He J, Yang M, Su C, "Dynamic Response Study of Space Large-Span Structure under Stochastic Crowd-Loading Excitation", Buildings, 14(5), 1203, 2024.
[8] Wu Y, Pan W, Luo Y, "Economical Design Comparison of Large-Span Composite Floor Systems with I Beams and Corrugated Web Beams", Buildings, 13(1940), 1940, 2023.
[9] Tsavdaridis K D, McKinley B, Kacaroglu B N, Corfar D-A, Lawson R M, "Bending test of long-span ultra-shallow floor beam (USFB) with two lightweight concretes", Structures, 66, 106895, 2024.
[10] Zhou X H, et al., "Experimental and analytical studies on the vibration serviceability of pre-stressed cable RC truss floor systems", Journal of Sound and Vibration, 361, 130 – 147, 2016.
[11] Han T, Liang S, Zhu X, et al., "Experimental study on the flexural behavior of large-span prestressed and steel-reinforced concrete slabs", Engineering Structures, 337, 120533, 2025.
[12] Huang L, Jie H, Zeng B, Zhou Z, Li L, "Experimental and numerical investigation on the mechanism of large-span floor system characterized by biaxially prestressed steel reinforced concrete beams", Structures, 69, 107443, 2024.
[13] Yang X, Wang, et al., "Experimental Study and Numerical Simulation on Mechanical Properties of the Bottom Plate in the Assembled Composite Slab with Additional Steel Trusses", Advances in Civil Engineering, 1 – 8, 2021.
[14] Liu J P, et al., "Vibration performance of composite steel-bar truss slab with steel girder", Steel and Composite Structures, 30(6), 577 – 589, 2019.
[15] Cao L, et al., "Experimental studies on vibration serviceability of composite steel-bar truss slab with steel girder under human activities", STEEL AND COMPOSITE STRUCTURES, 40(5), 663 – 678, 2021.
[16] Hu L, Ma, et al., "Research and application of U-shaped steel plate-concrete composite open-web sandwich slab structure with high strength bolts", Journal of Building Structures, 33(7), 61 – 69, 2012. (in Chinese)
[17] Luan H Q, et al., "Investigation on structural behavior of an innovative orthogonal-diagonal steel open-web sandwich floor system", Advances in Structural Engineering, 19(2), 353 – 371, 2016.
[18] Zhou X H, et al., "Experimental and analytical studies on the vibration serviceability of pre-stressed cable RC truss floor systems", Journal of Sound and Vibration, 361, 130 – 147, 2016.
[19] Qiao W T, et al., "EXPERIMENTAL STUDY ON THE FUNDAMENTAL MECHANICAL FEATURES OF CABLE-SUPPORTED RIBBED BEAM COMPOSITE SLAB STRUCTURE", Advanced Steel Construction: An International Journal, 13(2), 96 – 116, 2017.
[20] Qiao W T, et al., "Mechanical features of cable-supported ribbed beam composite slab structure", STEEL AND COMPOSITE STRUCTURES, 25(5), 523 – 534, 2017.
[21] Li M, Zhang J, Song B, et al., "Experimental and numerical investigation on flexural performance of non-prestressed concrete precast bottom slab with a removable section steel and three ribs", Structures, 79, 109441, 2025.
[22] An Q., Wang Y., "Spatial cable-supported floor system: ZL 201910759335.4" [Patent], 2019. (in Chinese)
[23] Ivanovic S, Pavic A, Reynolds P, "Vibration serviceability of footbridges under human-induced excitation: A literature review", Journal of Sound and Vibration, 279(1 – 2), 1 – 74, 2005.
[24] Belykh I, Bocian M, Champneys A R, et al., "Emergence of the London Millennium Bridge instability without synchronization", Nature Communications, 12, 2021.
[25] Lee S H, Lee K K, Woo S S, et al., "Global vertical mode vibrations due to human group rhythmic movement in a 39-story building structure", Engineering Structures, 57, 296 – 305, 2013.
[26] International Organization for Standardization, "ISO 10137: 2007. Bases for design of structures—serviceability of buildings and walkways against vibration", Geneva, Switzerland, 2007.
[27] Technical standard for vibration comfort of building floor structure: JGJ/T 441-2019, China Architecture and Construction Press, 2020. (in Chinese)
[28] Cao L, Liu, et al., "Experimental and analytical studies on the vibration serviceability of long-span prestressed concrete floor", Earthquake Engineering and Engineering Vibration, 17(2), 417–28, 2018.
[29] Liang H, Xie, et al., "Identification of Dynamic Parameters of Pedestrian Walking Model Based on a Coupled Pedestrian-Structure System", APPLIED SCIENCES-BASEL, 11(14), 6407, 2021.
[30] Fahmy Y G M, Sidky A N M, "An experimental investigation of composite floor vibration due to human activities. A case study", HBRC Journal, 8(3), 228–238, 2012.
[31] Zhang X, Wang, et al., "Experimental and Analytical Study on the Vibration Performance of U-Shaped Steel-Concrete Composite Hollow Waffle Slab", Shock & Vibration, 2020(1), 1–15, 2020.
[32] Brownjohn J M W, Pan T C, et al., "Floor Vibration Serviceability in a Multistory Factory Building", Journal of Performance of Constructed Facilities, 30(1), 1–14, 2016.
[33] Liu J P, Huang S, Li J, et al., "Vibration Serviceability of Large-span Steel–Concrete Composite Beam with Precast Hollow Core Slabs Under Walking Impact", Engineering, 19, 93–104, 2021.